

**Title:****Detection of Deterioration of Furnace Walls Using Large-Scale Point-Clouds****Authors:**

Yuki Shinozaki, yuki.shinozaki@uec.ac.jp, The University of Electro-Communications  
 Keisuke Kohira, keisuke.kohira@uec.ac.jp, The University of Electro-Communications  
 Hiroshi Masuda, h.masuda@uec.ac.jp, The University of Electro-Communications

**Keywords:**

Point-Cloud, Maintenance, Point Processing, Deterioration Diagnosis, Terrestrial Laser Scanner

**DOI:** 10.14733/cadconfP.2017.242-246

**Introduction:**

Blast furnaces are large industrial structures to produce iron. Since scaffolding and wearing of furnace walls are caused in their long-life cycle, furnaces have to be repeatedly renovated. In conventional diagnosis of furnaces, inspectors visually estimate the amount of scaffolding and wearing, and identify a need for maintenance. However, conventional diagnosis is strongly dependent on the skill of each inspector.

The state-of-the-art terrestrial laser scanners can capture dense point-clouds from large-scale facilities in a short time. They are promising to precisely estimate the amount of scaffolding and wearing of furnace walls. To obtain the amount of scaffolding and wearing, we have to estimate reference surfaces, which are the original wall shapes with no scaffolding and wearing.

However, in most cases, furnaces were not precisely built as designed in drawings even though most furnace walls were originally designed as a combination of nominal rotational surfaces, such as cylinders and cones. Therefore, when we suppose nominal surfaces for furnace walls, construction errors may be incorrectly detected as scaffolding or wearing parts.

Several researches have studied methods for extracting deterioration of large-scale facilities based on point clouds. Mizoguchi et al. [2] proposed a method for detecting wearing regions of bridge piers by supposing the original shapes as precise planes. They detected the aged deterioration as the difference between the ideal plane and the actual measured points. Their method is effective only when bridge piers are eroded largely, because actual shapes are not ideal planes. Nespeca et al. [3] also proposed a method for detecting scaffolding and wearing by calculating local planes. However, this method is very sensitive to kernel sizes, which have to be determined considering the delicate balance of the degree of wall distortion, the sizes of scaffolding and wearing, and noise levels of measured points.

In this paper, we discuss methods for detecting scaffolding and wearing on furnace walls using point-clouds. We introduce three different methods for calculating reference surfaces, and then evaluate these methods by comparing results of scaffolding and wearing.

**Extraction of Furnace Walls:**

In this research, point-clouds of a furnace were captured using a terrestrial laser scanner, FARO Focus 3D. The height of the furnace is about 30m. We measured the furnace inside the container at 12 positions. The total number of points is about 446 million. The point-clouds were registered using a commercial software, and each point-cloud was output in the PTX format, which stores 3D coordinates in the scanner-centered coordinate system with a registration matrix.

Fig. 1. shows a process to extract points on a furnace wall. In this paper, we assume that furnace walls consist of rotational surfaces. Fig. 1(a). shows point-clouds captured at 12 positions. Since the directions of laser beams are controlled by the azimuth angle  $\theta$  and the zenith angle  $\phi$ , scanner-centered coordinates  $(x, y, z)$  can be converted to spherical coordinates  $(r, \theta, \phi)$ , where the center of the sphere is the source of laser beams. Since points are ordered on the  $\theta$ - $\phi$  plane in a lattice manner, each point-cloud can be converted into a wireframe model by connecting adjacent points on the  $(\theta, \phi)$  plane. In this example, 12 wireframe models are generated for 12 point-clouds. Fig 1(b). shows converted wireframe models.

Then we place horizontal planes at equal intervals, as shown in Fig. 1(c)., and we calculate intersection points between each wireframe model and horizontal planes. Intersection points from each point-cloud are merged, as shown in Fig. 2. Then we detect circles on each horizontal plane using the RANSAC method, and estimate the center axis on which the most circle centers exist (Fig. 1(d)).

When sequential circles have approximately same radii, we regard them as a cylinder surface. The radius of the cylinder is estimated as the average of circle radii, as shown in Fig. 3(a). When radii of circles are linearly increased or decreased, we regard them as a cone, and calculate the taper of the cone, as shown in Fig. 3(b). These parameters are used as initial estimates of the reference surfaces.

In this research, we calculate the reference surfaces using intersection points in Fig. 2., and then calculate the amount of scaffolding and wearing as differences between the reference surfaces and measured points. To calculate the reference surfaces, we introduce three methods: (1) fitting to nominal surfaces, (2) fitting to a set of strip-like surfaces, and (3) fitting to constrained B-spline surfaces. In the following sections, we describe these methods.

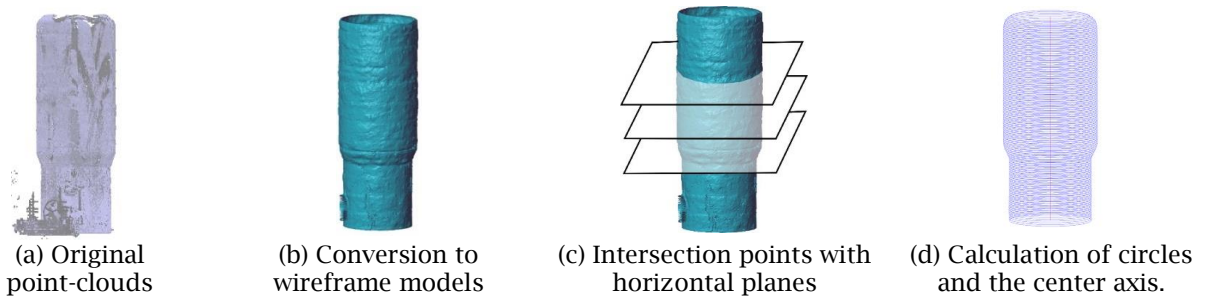


Fig. 1: Extraction of wall surfaces.

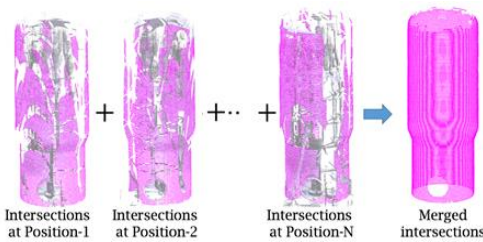


Fig. 2: Merging intersection points.

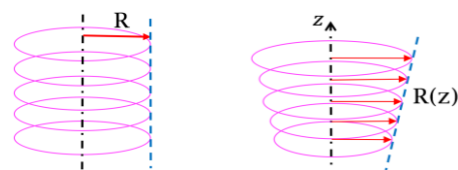


Fig. 3: Initial estimate of furnace wall.

**Reference Surfaces by Nominal Cylinders and Cones:**

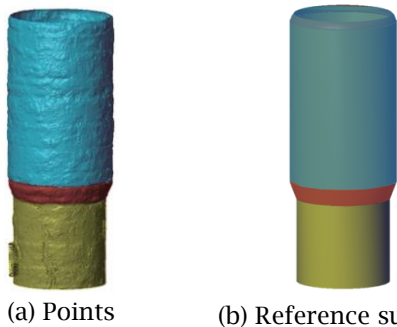
Furnace walls are typically designed as rotational surfaces. The furnace wall in Fig. 4. was originally designed as two cylinders and a cone. First, in order to indicate that the original shape is largely distorted from the nominal rotating body, we fit cylinders and a cone to intersection points using the faithful least-squares fitting [1]. In this method, we denote the parameter of a cylinder or a cone as  $\mathbf{s}$ , the modified distance function proposed by Lucacs, et. al. [1] as  $d(\mathbf{s}, \mathbf{p}_i)$ , and measured points on the surface as  $\{\mathbf{p}_i\}$  ( $i \in A$ ). Then the surface equation can be calculated by:

$$\underset{\mathbf{s}}{\operatorname{argmin}} \sum_{i \in A} d(\mathbf{s}, \mathbf{p}_i)^2 \tag{3.1}$$

Fig. 4 shows two cylinders and a cone, which were calculated as reference surfaces.

Then we calculate differences between the reference surfaces and measured points. We represent points on the surface as  $(\theta, \xi)$ , as shown in Fig. 5. We define an image on the  $\theta$ - $\xi$  plane, and describe differences between the nominal surface and measured points on each pixel. When multiple points are mapped onto the same pixel, the smallest difference is stored on the pixel. In the difference map in Fig. 5, differences are visualized using RGB colors. Red color pixels show wearing, blue color pixels show scaffolding, and green color pixels show regions with no wearing and scaffolding.

In Fig. 6(a), large red and blue areas alternately appear. This is because the actual furnace wall is not a precise rotational surface, as shown in Fig. 6(b), and distortion of the as-built wall was detected instead of wearing and scaffolding areas. This example shows that the as-built shape is rather different from drawings, and the difference is larger than the amount of wearing and scaffolding. From this result, we can conclude that it is not reasonable to approximate actual furnace shapes as rotating bodies.



(a) Points (b) Reference surfaces  
Fig. 4: Fitting nominal cylinders and a cone.

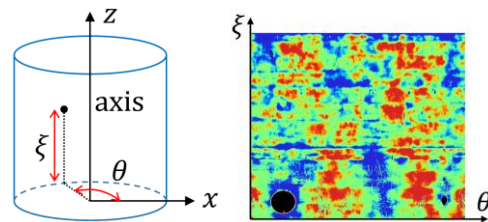
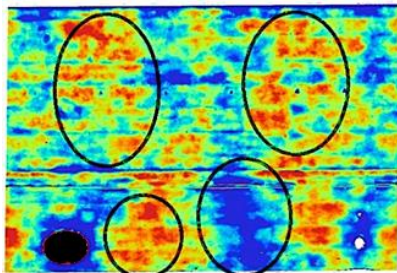
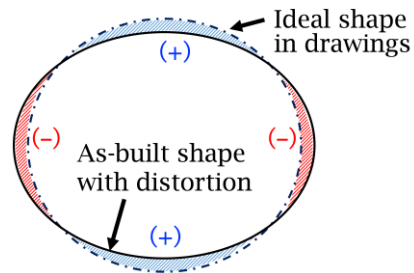


Fig. 5: Difference Map.



(a) Difference map.



(b) Difference between designed and built shapes.

Fig. 6: Difference map by nominal reference surfaces.

Reference Surfaces by Subdivided Strip Surfaces:

In the next step, we approximate a furnace wall using a set of strips of cylinders or cones to represent distorted walls, as shown in Fig. 7(a). In this method, points  $\{\mathbf{p}_i\}$  on the wall are segmented in a strip manner, and points on each strip are represented using different surfaces. We denote points on strip  $k$  as  $\{\mathbf{p}_j\}$  ( $j \in A_k$ ). To avoid discontinuity at the border of strips, we define overlapping strips, as shown in Fig. 7(b).

However, surface fitting to a small range of surfaces is unstable, because cylinders and cones are calculated using non-linear optimization [1]. Thus, we calculate each surface using all points, but add large weights  $w$  to points on a strip, as shown in Fig. 8. The parameters  $\mathbf{s}_k$  of the surface of strip  $k$  are calculated using the following equation:

$$\operatorname{argmin}_{\mathbf{s}_k} \left[ w \sum_{i \in A_k} d(\mathbf{s}_k, \mathbf{p}_i)^2 + \sum_{i \notin A_k} d(\mathbf{s}_k, \mathbf{p}_i)^2 \right] \quad (w \gg 1) \tag{4.1}$$

A surface equation is calculated for each strip-like segment. Then we calculate a difference map by mapping differences between strip-like reference surfaces and measure points on the  $\theta$ - $\xi$  plane, as defined in Fig. 5. Differences in overlapping regions are linearly blended. Suppose that strip  $a$  and strip  $b$  overlap as shown in Fig. 8(a),  $l_a$  and  $l_b$  are the distances of the black pixel from the borders of strips, and  $\delta_a$  and  $\delta_b$  are difference values on the pixel. Then the difference value  $\delta$  is calculated as:

$$\delta = \frac{l_a \delta_b + l_b \delta_a}{l_a + l_b} \quad (4.2)$$

Fig. 8(b) shows a difference map, which were blended using overlapping strips. In this method, a reasonable difference map could be calculated. However, large red regions are generated at the upper parts of the cylinder, as shown in the circle in Fig. 8(b). This is because points are relatively sparse at far distances from the laser scanner, and reference surfaces are not well fitted to sparse regions.

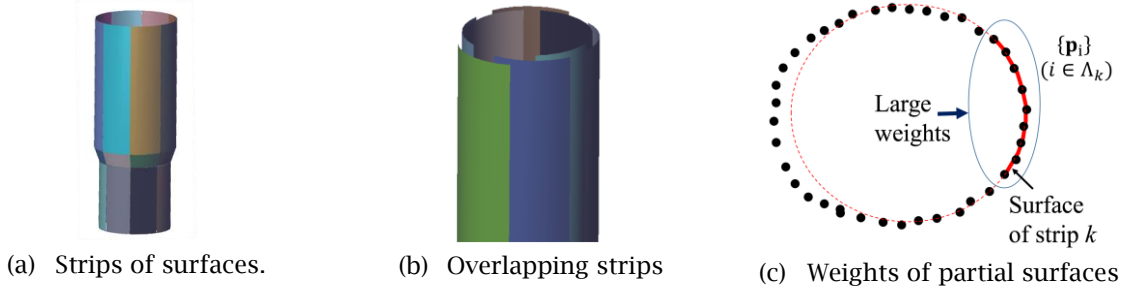


Fig. 7: Strips of cylinders and cones.

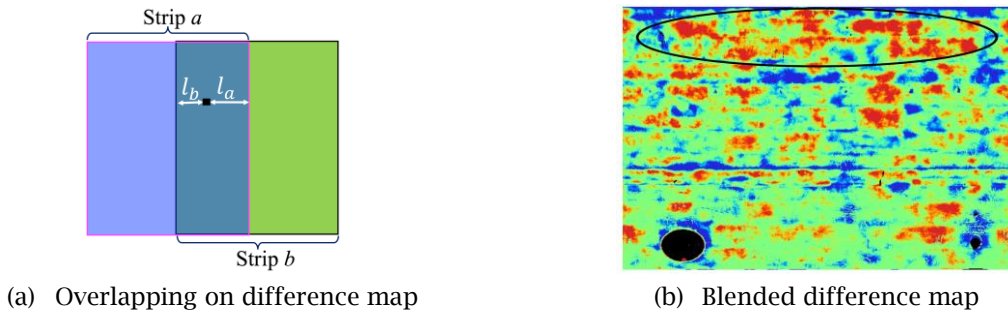


Fig. 8: Difference map based on strip-like surfaces.

#### Reference Surfaces by Constrained B-Spline Surfaces:

While distortion of as-built furnace walls is relatively global, scaffolding and wearing tend to appear as local bumps. Therefore, we consider multi-resolution B-spline surfaces to extract the base surfaces for reference surfaces, and detail surfaces for scaffolding and wearing.

To calculate a B-spline surface, we convert  $(x, y, z)$  coordinates into cylindrical coordinates  $(\theta, \zeta, r)$ , as shown in Fig. 9(a). Then the furnace wall can be represented as approximately planar surfaces, as shown in Fig. 9(b), because it is approximately a rotational surface. We segment the converted surface into a set of planar regions using the RANSAC method. A B-spline surface is fitted to each planar region.

We suppose that  $\mathbf{S}(u, v)$  is a B-spline surface;  $\{\mathbf{q}_{ij}\}$  are the control points;  $m_u$  and  $m_v$  are the numbers of control points in  $u$  and  $v$  directions;  $\{\mathbf{p}_i\}$  ( $i = 1, \dots, n$ ) are measured points. Parameters  $(u_i, v_i)$  of  $\mathbf{p}_i$  are specified as  $(\theta, \zeta)$  of point  $\mathbf{p}_i$  on the  $\theta$ - $\zeta$  plane.

In laser scanning, points are partially missing because of holes on furnace walls and occluded regions. Then, control points of B-spline surfaces become indeterminate in missing regions. Therefore, we add curvature terms to the objective function. In this paper, we simply represent curvature terms as linear equations, because rotational surfaces are converted to flat planes in our method.

Then we minimize the following function to obtain B-spline surfaces. The second term represents simplified curvature. The weight  $\lambda$  should be a small value. In this research, we specified  $\lambda = 10^{-4}$ .

$$\sum_{i=1}^n |\mathbf{S}(u_i, v_i) - \mathbf{p}_i|^2 + \frac{n\lambda}{m_u m_v} \left\{ \sum_{i=1}^{m_u-2} \sum_{j=1}^{m_v} |\mathbf{q}_{i,j} - 2\mathbf{q}_{i+1,j} + \mathbf{q}_{i+2,j}|^2 + \sum_{i=1}^{m_u} \sum_{j=1}^{m_v-2} |\mathbf{q}_{i,j} - 2\mathbf{q}_{i,j+1} + \mathbf{q}_{i,j+2}|^2 \right\} \quad (5.1)$$

To obtain scaffoldings and wearing, we calculate two B-spline surfaces. One has a small number of control points to extract the base surface, and the other has a lot of control points to represent the detail surface. A difference map is generated as the difference between the base surface and the detail surface. Fig. 10. shows the difference map. In this result, questionable large red or blue regions disappeared from the upper regions. This method is robust to differences of point density.

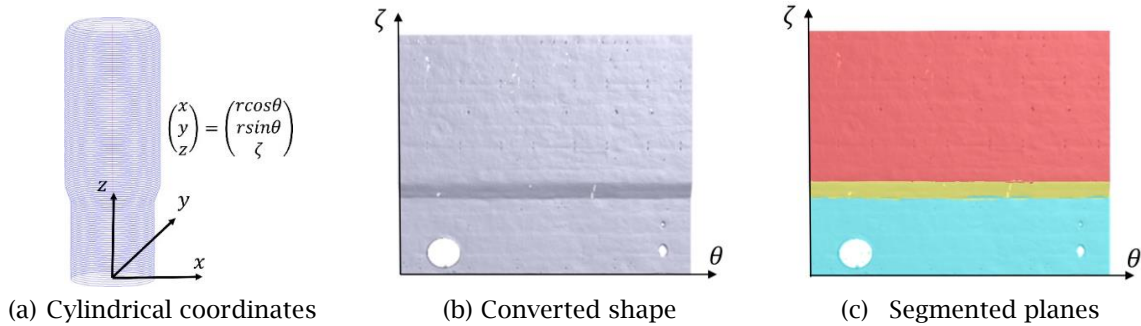


Fig. 9: Difference map based on strips of surfaces.

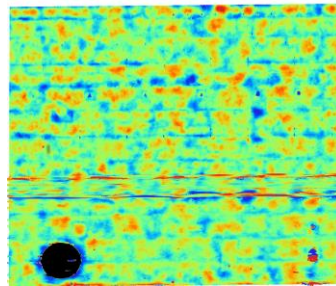


Fig. 10: Difference map based on B-Spline surfaces.

### Conclusion:

In this paper, we proposed methods for diagnosing scaffolding and wearing of furnace walls. We calculated reference surfaces of the furnace wall using three methods. When we fitted nominal cylinders and cones, scaffolding and wearing regions could not be properly identified. When we fitted a set of strip-like surfaces, scaffolding and wearing could be extracted, but the result was sensitive to differences of point density. Finally, we calculated scaffolding and wearing regions using low and high resolutions of B-spline surfaces. The result was the best in the three methods. In future work, we would like to investigate ground truth of scaffolding and wearing and validate accuracy of our method.

### References:

- [1] Lukács, G.; Martin, R.; Marshall D.: Faithful least-squares fitting of spheres, cylinders, cones and tori for reliable segmentation, European Conference on Computer Vision, Springer Berlin Heidelberg, 1998.
- [2] Mizoguchi, T.; Koda, Y.; Iwaki, I.; Wakabayashi, H.; Kobayashi, Y.; Shirai, K.; Lee, H. S.: Quantitative Scaling Evaluation of Concrete Structures Based on Terrestrial Laser Scanning, Automation in Construction, 35, 263-274. <http://dx.doi.org/10.1016/j.autcon.2013.05.022>
- [3] Nespeca, R.; De Luca, L.: Analysis, Thematic Maps and Data Mining from Point Cloud to Ontology for Software Development, ISPRS-International Archives of the Photogrammetry, Remote Sensing and Spatial Information Sciences 2016, 347-354. DOI:10.5194/isprs-archives-XLI-B5-347-2016